Journal of Biomechanics 174 (2024) 112212

Contents lists available at ScienceDirect

Journal of Biomechanics

journal homepage: www.elsevier.com/locate/jbiomech

Impact of hypertension and arterial wall expansion on transport properties and atherosclerosis progression

Patricia Hernández-López [a,*], Nicolás Laita [a], Myriam Cilla [a,b], Miguel Ángel Martínez [a,b], Estefanía Peña [a,b]

[a] Aragón Institute of Engineering Research (I3A). University of Zaragoza, Spain
[b] Biomedical Research Networking Center in Bioengineering, Biomaterials and Nanomedicine (CIBER-BBN), Spain

ARTICLE INFO

Keywords:
Atherosclerosis
Mechanobiological model
Mechanical expansion
Porosity
Permeability
Hyperelastic material
Carotid artery

ABSTRACT

This study explored the impact of hypertension on atheroma plaque formation through a mechanobiological model. The model incorporates blood flow via the Navier–Stokes equation. Plasma flow through the endothelium is determined by Darcy's law and the Kedem–Katchalsky equations, which consider the three-pore model utilized for substance flow across the endothelium. The behaviour of these substances within the arterial wall is described by convection–diffusion–reaction equations, while the arterial wall itself is modelled as a hyperelastic material using Yeoh's model. To accurately evaluate hypertension's influence, adjustments were made to incorporate wall compression-induced wall compaction by radial compression. This compaction impacts three key variables of the transport phenomena: diffusion, porosity, and permeability.

Based on the obtained findings, we can conclude that hypertension significantly augments plaque growth, leading to an over 400% increase in plaque thickness. This effect persists regardless of whether wall mechanics are considered. Tortuosity, arterial wall permeability, and porosity have minimal impact on atheroma plaque growth under normal arterial pressure. However, the atheroma plaque growth changes dramatically in hypertensive cases. In such scenarios, the collective influence of all factors—tortuosity, permeability, and porosity—results in nearly a 20% increase in plaque growth. This emphasizes the importance of considering wall compression due to hypertension in patient studies, where elevated blood pressure and high cholesterol levels commonly coexist.

1. Introduction

Cardiovascular diseases (CVDs) continue to pose a significant threat to global health, being a leading cause of morbidity and mortality worldwide (Virani et al., 2021). Among various cardiovascular pathologies, atherosclerosis is a significant contributor to the burden of CVDs (Caro et al., 1978; Wang and Patterson, 2015). Atherosclerosis is a chronic inflammatory disease characterized by the accumulation of fatty deposits, cholesterol, cellular waste, and other substances on the arterial inner layer. This substances accumulation progressively narrows and stiffens arteries, impeding blood flow (Humphrey, 2002).

Several factors contribute to atherosclerosis, including endothelial damage that increases arterial wall permeability, changes in endothelial cell morphology due to haemodynamic factors, and elevated levels of low-density lipoproteins (LDL) in the bloodstream (Gusev and Sarapultsev, 2023). Despite extensive research, the mechanisms underlying this condition remain partially understood. Thus, studying atheroma plaque formation and understanding the influence of mechanical stimuli on their growth and localization is crucial. Predicting vulnerable plaque sites and developing early detection or prevention strategies could significantly mitigate disease progression.

Due to an increase in the endothelial permeability, bloodstream substances such as plasma and LDL molecules are able to cross the endothelium and infiltrate the arterial wall (Humphrey, 2002). Once LDL molecules penetrate the arterial wall, they become isolated from antioxidants in the bloodstream, leading to oxidation and the formation of oxidized LDL (Libby and Aikawa, 2002). Oxidized LDL can interact with surrounding tissues, causing damage and triggering an immune response that attracts monocytes from the bloodstream into the arterial wall (Humphrey, 2002). Within the arterial wall, monocytes seek to remove oxidized LDL molecules, leading to macrophages differentiation in response some specific arterial wall proteins. Macrophages play a crucial role in clearing oxidized LDL through phagocytosis, during which they release cytokines. When macrophages can no longer ingest

* Corresponding author.
E-mail address: phernand@unizar.es (P. Hernández-López).

https://doi.org/10.1016/j.jbiomech.2024.112212
Accepted 27 June 2024
Available online 9 July 2024
0021-9290/© 2024 The Author(s). Published by Elsevier Ltd. This is an open access article under the CC BY-NC license (http://creativecommons.org/licenses/by-nc/4.0/).

oxidized LDL, they eventually transform into foam cells, contributing to the lipid core of the plaque (Bentzon et al., 2014).

On the other hand, the impact of blood pressure variability on atherosclerosis plaques is an important multifaceted aspect of cardiovascular health. Elevated blood pressure can lead to endothelial damage, increased of wall deformations, permeability and porosity, fostering conditions conducive to atherosclerotic plaque formation (Liu et al., 2022). This adds further complexity to the relationship between blood pressure and atherosclerosis.

Given the severe consequences of advanced atherosclerosis (VanEpps and Vorp, 2007), it is vital to develop tools for early disease prediction. Numerous studies have focused on investigating the atherosclerotic process to anticipate early detection (Sun et al., 2007; Dabagh et al., 2009). In this regard, computational modelling has become a widely used tool to simulate various pathological scenarios and predict potential outcomes (Cilla et al., 2012, 2013; Hernández-López et al., 2021, 2023; Olgac et al., 2008; Cunningham and Gotlieb, 2005; Filipovic et al., 2013; Ogunrinade et al., 2002). The etiology of atherosclerosis involves multiple factors, such as haemodynamic stimuli from blood flow against the arterial wall (Bulelzai and Dubbeldam, 2012) and, although extensive research into the complex interplay of these factors in plaques formation, many aspects remain unclear (Elishaev et al., 2022). Typically, these models depict an undamaged vessel where transport phenomena is governed by diffusion, convection, and reaction within the surrounding wall layers, often overlooking the impact of mechanical deformation on substances transport (Schwenke and Carew, 1989; Weinbaum et al., 1985; Chien, 2003; Brown et al., 2016).

Limited research has been conducted to investigate the influence of hypertension on LDL passage across the arterial wall. In an experiment by Meyer et al. (1996), LDL flux across the arterial wall was measured at different intraluminal pressures, showing a consistent increase in LDL flux at higher pressure levels. To study LDL movement under hypertension, Dabagh et al. (2009) introduced a multilayered model of the aortic wall, considering the effects of increased endothelial cell turnover and intimal deformation under increased pressure. Their results indicated that hypertension indirectly increases LDL accumulation in the subendothelial layers, leading to intimal compaction and promoting endothelial cell turnover, potentially causing gradual LDL accumulation within the intima. Sun et al. (2007) performed numerical evaluations of hypertension's effect on LDL concentration within the arterial wall, finding that increased transversal pressure not only increases endothelial cell permeability, allowing greater wall permeation, but also increases the permeability of the outer layer. These studies assess hypertension's effect on LDL accumulation, but none specifically analyse the resultant wall growth due to the inflammatory process. Only Dabagh et al. (2009) includes the effect of wall compaction due to hypertension and its effect on wall transport properties and LDL profile along the artery.

Within the development of computational models to simulate atheroma plaque growth and understand the progression of atherosclerosis, two primary modelling approaches are commonly found: continuous models such as Cilla et al. (2013) or Ai and Vafai (2006) and agent-based models (ABMs) such as Olivares et al. (2016) or Pappalardo et al. (2008). Both approaches offer distinct methodologies and insights. Continuous models use differential equations to represent the changes in concentrations of substances such as LDL within arterial walls over time. They assume a continuous distribution of variables, capturing macroscopic dynamics of plaque growth effectively. The primary advantages of continuous models include (i) mathematical tractability: which allows for the use of established mathematical techniques and theories to derive analytical solutions or implement efficient numerical methods. Additionally, as they are based on differential equations, their (ii) computational efficiency enables relatively quick solutions, even for complex scenarios, which is crucial for simulating long-term plaque development. Continuous models are also efficient at (iii) generalization, as they can easily incorporate a wide range of biological processes and interactions, such as LDL diffusion, chemical reactions, and mechanical forces. This flexibility allows for modelling different aspects of plaque growth under varying physiological conditions. Furthermore, these models facilitate (iv) parameter sensitivity analyses, helping to identify key parameters and their influence on plaque development. This can guide experimental design and enhance the understanding of underlying mechanisms.

In contrast, ABMs simulate individual agents' behaviours and interactions, such as cells or molecules, following rules that can lead to complex system behaviours from simple interactions. ABMs are particularly useful for (i) heterogeneity and stochasticity as they successfully capture the inherent variability and randomness in biological systems, essential for processes like cellular interactions and discrete events of LDL oxidation and macrophage recruitment. They also provide (ii) detailed spatial information, enabling the study of localized phenomena like micro-domain formation within plaques or heterogeneous distribution of chemical species. Additionally, ABMs can model (iii) detailed interactions between individual agents, which is valuable for studying processes involving direct cell–cell or cell–molecule interactions. Despite their advantages, ABMs can be computationally intensive, especially when simulating large populations of agents over extended periods. The complexity of rule-based interactions in ABMs can also complicate the derivation of general principles or to perform comprehensive sensitivity analyses. Given these considerations, we selected a continuous models for this study due to their scalability, robustness, predictability, and ability to simplify complex interactions.

In this study, we present the most comprehensive investigation to date of how arterial mechanical expansion affects the transport properties of an arterial wall in both normal and hypertensive conditions. Extending a previously established computational model by the same authors (Hernández-López et al., 2023, 2021), our study integrates a mechanical framework to investigate the role of hypertension on atheroma plaque growth. Furthermore, our model incorporates state-of-the-art descriptions of arterial tissue mechanical properties using a hyperelastic material model. We establish correlations between mechanical strain during inflation and changes in diffusion within the arterial wall.

2. Materials and methods

2.1. Mechanical model

2.1.1. Modelling the arterial wall

The model comprises the arterial lumen and wall, represented as a monolayered structure. The endothelium and adventitia are modelled as membranes within this structure. The arterial wall is described using the Yeoh strain energy density function for compressible, isotropic and hyperelastic materials (Yeoh, 1993):

$$\Psi = \sum_{i=1}^{3} C_{Yeoh,i} \cdot \left[I_1 - 3\right]^i + \frac{1}{2} \cdot K_w (1 - J)^2, \tag{1}$$

where I_1 the first invariant of the right Cauchy–Green deformation tensor. $C_{Yeoh,i}$ are material constants determined from experimental data. The initial compression modulus of the arterial wall, K_w, is also defined. Studies such as Nolan and McGarry (2016) indicate that the arterial wall is not fully incompressible and exhibits a mean volumetric variation, J, of 9.31%. K_w was then fitted to satisfy this experimental volumetric variation at the start of the simulations ($K_w = 4.46 \cdot 10^4$ Pa). The model parameters were calibrated against the experimental data reported by Holzapfel et al. (2005), as shown in Table 1.

As boundary conditions, both ends of the model were fixed along the longitudinal axis of the artery to prevent movement as a rigid solid. Additionally, the adventitia is fixed along the radial axis to prevent deformation due to blood flow pressure.

Table 1
List of constants of the Yeoh's model in the arterial wall fitted from Holzapfel et al. (2005).

Parameter	Value (kPa)
$C_{Yeoh,1}$	17.005
$C_{Yeoh,2}$	−73.424
$C_{Yeoh,3}$	414.952

2.1.2. Derivation of arterial diffusion coefficients as a function of deformation

As mentioned above, the arterial wall has been modelled as a porous medium through which different substances advance by diffusion and convection mechanisms. Diffusion processes are strongly dependent on the deformation of the blood vessel, which hinders the diffusion of substances (Denny et al., 2012; Denny and Walsh, 2014). In this way, tortuosity provides an idea of the diffusion difficulty of different substances in the arterial wall (see Fig. 1).

The tortuosity of the blood vessel at the initial state is defined as

$$\boldsymbol{\tau_0} = \frac{L}{x}, \tag{2}$$

where x is the wall thickness and L the particle path length, (Fig. 1.a). It should be noted that this equation is a reasonable approximation, but it does not assure that the length of the particle path L remains constant after the deformation.

Then, the effective coefficient diffusion can be defined as

$$D_{effecive} = \frac{\boldsymbol{\epsilon}}{\boldsymbol{\tau}} D \tag{3}$$

where ϵ is the porosity of the arterial wall, τ is the tortuosity and D is the substance diffusion coefficient in a free medium.

However, the arterial wall is compressed and deformed by the blood pressure. When compressed, the thickness of the wall is modified (see Fig. 1.b) and the tortuosity can be rewritten as

$$\boldsymbol{\tau} = \frac{L}{x - \Delta x}, \tag{4}$$

where Δx is the wall thickness compression.

The radial deformation can be described as $\varepsilon_r = \frac{\Delta x}{x}$, assuming negative Δx for compression. Then,

$$\boldsymbol{\tau} = \frac{\frac{L}{x}}{\frac{x}{x} - \frac{\Delta x}{x}} = \frac{\boldsymbol{\tau_0}}{1 + \boldsymbol{\varepsilon_r}}, \tag{5}$$

and

$$D_{effecive} = \frac{\boldsymbol{\epsilon}(1 + \varepsilon_r)}{\boldsymbol{\tau_0}} D \tag{6}$$

The considered diffusion coefficients were obtained experimentally (Prosi et al., 2005; Budu-Grajdeanu et al., 2008), so they already take into account the initial tortuosity and tissue porosity based on real diffusion data in arterial tissue. Therefore, the equation for the initial and effective diffusion coefficients can be rewritten as follows:

$$D_{initial} = \frac{\boldsymbol{\epsilon}}{\boldsymbol{\tau_0}} D \qquad D_{effective} = (1 + \varepsilon_r) D_{initial} \tag{7}$$

Due to the natural structure of the arterial wall, the diffusion coefficient is anisotropic, with longitudinal diffusion being three times greater than radial diffusion ($\varepsilon_z = 3\varepsilon_r$) (Yuan et al., 1991). Taking all this into account, the diffusion coefficients of the different substances and cells considered accordingly:

$$D_{effective} = \begin{pmatrix} (1 + \varepsilon_r) D_{initial} & 0 \\ 0 & 3(1 + \varepsilon_r) D_{initial} \end{pmatrix} \tag{8}$$

It should be noted that the inclusion of tortuosity only affects the diffusion coefficients of LDL, oxidized LDL, monocytes and macrophages. The diffusion of other cells and substances along the arterial wall is not considered.

2.1.3. Derivation of arterial porosity as a function of deformation

According to the pore theory, the arterial wall consists of a matrix comprising proteoglycans and collagen. This proteoglycan matrix is composed of core proteins, glycosaminoglycan fibres, and elongated central filaments of hyaluronic acid (Dabagh et al., 2009).

The porosity of the intima is calculated as the product of the porosity of the proteoglycan (ϵ_{pg}) and collagen matrix ϵ_{cg}. According to Huang et al. (1994, 1992), the porosity of the matrix of proteoglycans ϵ_{0pg} is equal to 0.98875. However, the deformation due to the arterial flow pressure should be included, so the porosity of the proteoglycan matrix (ϵ_{pg}) can be obtained as

$$\epsilon_{pg} = 1 - \frac{L_0}{L_i}(1 - \epsilon_{0pg}), \tag{9}$$

where L_0 and L_i are uncompressed and compressed intima thickness, respectively.

The porosity of the collagen matrix ϵ_{cg} is calculated similarly to the porosity of the proteoglycan, but considering a ϵ_{0cg} of 0.95 (Huang et al., 1998; Truskey et al., 1992), since collagen accounts for approximately 5% of the intima at zero pressure.

On the other hand, the partition coefficient of the intima ($\boldsymbol{\Phi}_i$) is affected when the porosity varies (Dabagh et al., 2009). This coefficient is defined as the ratio of the pore area available for solute transport to the total pore area:

$$\boldsymbol{\Phi}_i = exp[-(1-\epsilon_{pg})(2\frac{r_s}{r_{pg}} + \frac{{r_s}^2}{{r_{pg}}^2})](\epsilon_{cg} + \epsilon_{pg} - 1) exp[1(1-\epsilon_{cg}^{\frac{1}{2}})(1 + \frac{r_s}{r_{cg}})], \tag{10}$$

where r_s is the radius of the solute (LDL). r_{cg} is the collagen fibres radius (20 nm) and r_{pg} the proteoglycan matrix radius (2.313 nm). It should be noted that the LDL solute lag coefficient ($klag$) will be modified as it depends on the partition coefficient as follows (Dabagh et al., 2009).

$$klag = \frac{2 - \boldsymbol{\Phi}_i}{2}. \tag{11}$$

2.1.4. Derivation of arterial permeability as a function of deformation

In this case, we introduce the dependence of wall mechanics through permeability. Again, the pore theory is used, and the permeability coefficient of the wall is calculated by considering the proteoglycan matrix and the collagen in parallel.

According to Jesionek et al. (2016), the hydraulic permeability of the intima can be defined as

$$\frac{1}{K_{intima}} = \frac{1}{K_{pg}} + \frac{1}{K_{cg}}, \tag{12}$$

where K_{intima}, K_{pg} and K_{cg} are the intima, proteoglycan matrix and collagen permeabilities, respectively.

Using the Carman–Kozeny equation (Curry and Michel, 1980; Jesionek et al., 2016), the specific permeabilities K_{pg} and K_{cg} can be calculated.

$$K_{pg} = \frac{r_{pg}^2 \epsilon_{pg}^3}{4G(1 - \epsilon_{pg}^2)} \qquad \text{and} \qquad K_{cg} = \frac{r_{cg}^2 \epsilon_{cg}^3}{4G(1 - \epsilon_{cg}^2)} \tag{13}$$

where G is the Kozeny constant, expressed for uncharged cylindrical randomly arranged fibres as (Huang et al., 1998)

$$G = \frac{2}{3} G_r + \frac{1}{3} G_p \tag{14}$$

where G_r and G_p refer to the flow perpendicular and parallel to the fibres, respectively.

$$G = \frac{2}{3} \frac{2\epsilon^3}{(1-\epsilon)[2ln(\frac{1}{1-\epsilon}) - 3 + 4(1-\epsilon) - (1-\epsilon^2)]} + \frac{1}{3} \frac{2\epsilon^3}{(1-\epsilon)[ln(\frac{1}{1-\epsilon}) - \frac{1-(1-\epsilon)^2}{1+(1-\epsilon)^2}]}, \tag{15}$$

being the value of ϵ equals to ϵ_{gp} for the K_{pg} equation and ϵ_{cg} for the K_{pg} equation. The expressions of ϵ_{gp} and ϵ_{cg} are those used to derive arterial porosity as a function of deformation (previous section).

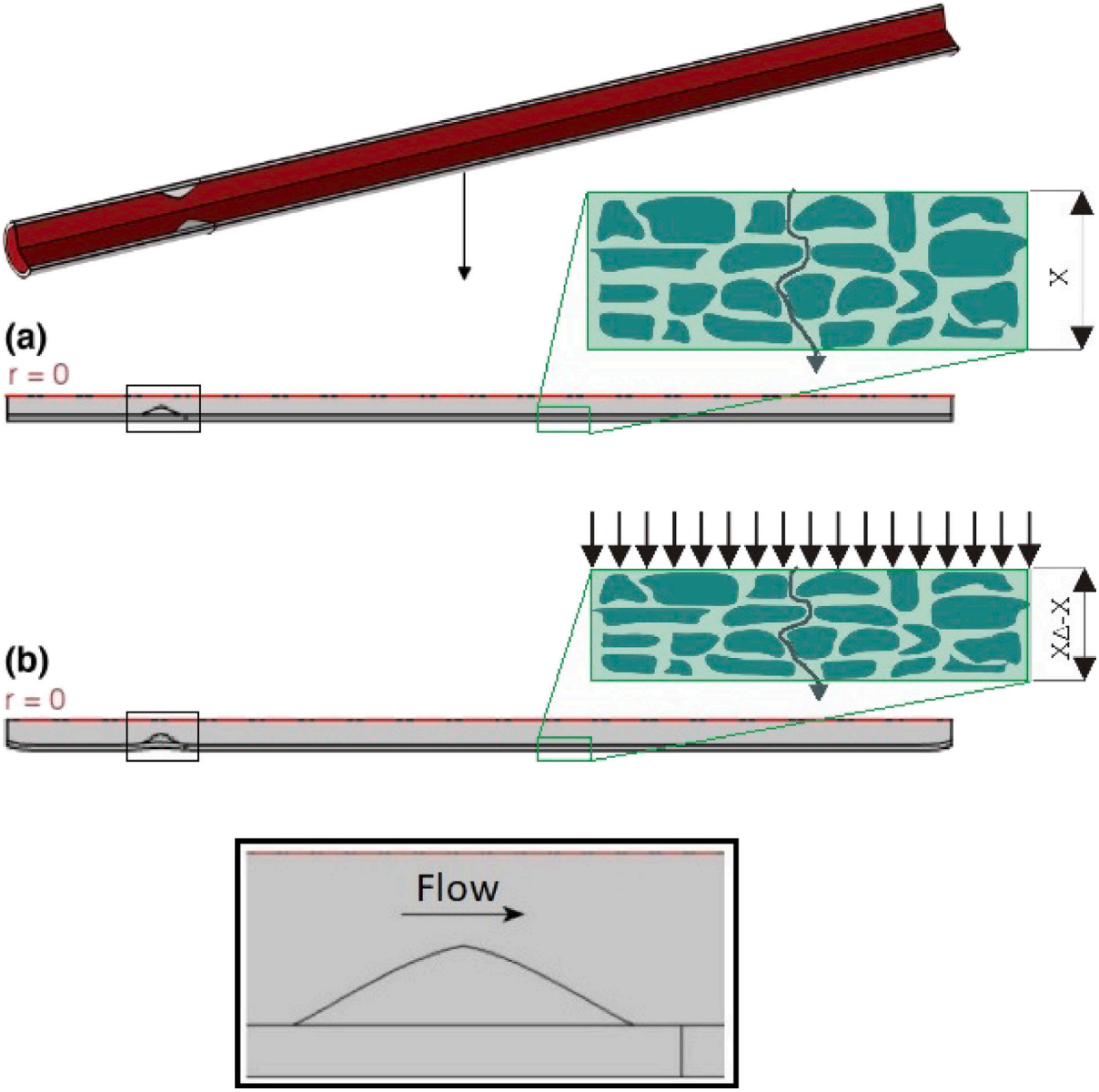

Fig. 1. Two-dimensional axisymmetric geometry composed of lumen, the arterial wall, and obstacle plaque. (a) Zero-pressure geometry and (b) Pressurized geometry. The Figure also included a schematic illustration about the influence of wall expansion on tortuosity.

2.2. Inflammatory model

This section outlines the mathematical model, summarizing equations relating to various aspects such as blood flow in the lumen, plasma flow across the endothelium, inflammatory processes in the arterial wall, and plaque growth. The full set of equations and parameters can be found in the mechanobiological models proposed by Hernández-López et al. (2021) upon which this study is based.

2.2.1. Pressure blood flow

Blood flow within the arterial lumen is characterized as laminar (we consider a Reynolds number, Re, of approximately 950 for the mean arterial diameter under physiological conditions Malvè et al., 2014). Blood is also treated as a Newtonian incompressible fluid due to lumen diameters in arteries is greater than 0.5 mm (Caro et al., 1978; Perktold et al., 1991). Lastly, is also modelled as a homogeneous fluid due to the negligible size of particles relative to the arterial lumen diameter (Malvè et al., 2014). The governing equations for blood flow within the lumen are the Navier–Stokes and continuity equations (16).

$$\rho_b \frac{\partial \boldsymbol{u_b}}{\partial t} + \rho_b(\boldsymbol{u_b} \cdot \nabla)\boldsymbol{u_b} = \nabla \cdot [-P_b \boldsymbol{I} + \mu_b(\nabla \boldsymbol{u_b} + (\nabla \boldsymbol{u_b})^T)]$$
$$\rho_b \nabla \cdot \boldsymbol{u_b} = 0, \tag{16}$$

where the subscript b refers to blood, so the parameters ρ_b and μ_b are the density and dynamic viscosity of blood respectively, while $\boldsymbol{u_b}$ and P_b are the velocity and pressure of blood flow in the lumen.

Due to the computational cost involved in performing coupled inflation calculations with transient blood flow (dependent on the cardiac cycle), and since the study focuses on wall mechanics influence rather than blood flow issues, the simulation assumes steady-state blood flow, with wall shear stress (WSS) as the primary haemodynamic stimulus. The inlet velocity is prescribed according to the Hagen–Poiseuille profile defined by Olgac et al. (2008), while the outlet pressure is set to 100 mmHg and 160 mmHg for the normal and hypertensive environments, respectively.

2.3. Plasma flow

Due to the porous structure of the arterial wall, plasma is able to enter the bloodstream, resulting in plasma flow across the endothelium. This flow is described by Darcy's law in conjunction with continuity equations (Olgac et al., 2008; Huang and Tarbell, 1997; Sun et al., 2007). Darcy's Law establishes a relationship between the velocity of plasma flow and the pressure drop across the arterial wall, taking into account parameters associated with its porous nature such as permeability (k_w) and the dynamic viscosity (μ_p).

$$\boldsymbol{u_p} = -\frac{k_w}{\mu_p}\nabla P_p, \tag{17}$$

Plasma flow across the endothelium, which is calculated using the Kedem–Katchalsky equations (Kedem and Katchalsky, 1958) and the three-pore model (Olgac et al., 2008), is entirely due to convection, see Appendix A.

$$\frac{\partial(\epsilon_w \rho_p)}{\partial t} + \nabla \cdot (\rho_p \boldsymbol{u_p}) = \boldsymbol{J}_v, \tag{18}$$

The boundary conditions for plasma flow across the endothelium include the normal velocity of plasma flow and the pressure in the adventitia, affecting material flow and plaque size (Hernández-López et al., 2021).

2.4. Substance flow across the endothelium

Blood contains many molecules and cells, including LDL and monocytes. LDL and monocytes are carried by blood flow through the arterial lumen, and their transport is governed by convection–diffusion equations within the lumen:

$$\underbrace{\frac{\partial C_i}{\partial t}}_{Time} + \underbrace{\nabla \cdot (-D_i \nabla C_i)}_{Diffusion} + \underbrace{\boldsymbol{u_b} \cdot \nabla C_i}_{Convection} = 0 \tag{19}$$

A high LDL concentration in the blood is assumed according to a pathological model (2.7 $\frac{\text{mg}}{\text{m}^3}$ (Cilla et al., 2013), equivalent to 6.98 $\frac{\text{mol}}{\text{m}^3}$). Additionally, we impose a physiological luminal monocyte inlet concentration of 550×10^{-9} $\frac{\text{cells}}{\text{m}^3}$ (Sun et al., 2007). The flow of LDL and monocytes is considered through the endothelium, as they are the only substances considered that are present in the bloodstream. The LDL flow depends on the three-pore model and the monocyte flow is modelled with a stimulus-dependent sigmoid function (Cilla et al., 2013). An increase in both influx concentrations would result in an escalation of plaque growth.

The flow of substances across the arterial wall, N_i can be defined as:

$$\boldsymbol{N_i} = -D_i \nabla C_i + \boldsymbol{u_p} C_i, \tag{20}$$

where the first is due to diffusion and second one to convection. As with plasma flow, LDL flow (J_s) across the endothelium can be modelled using the three-pore model, see Appendix B.

2.5. Inflammatory process

The inflammatory process within the arterial wall involves a variety of substances. In our model, we include molecules such as LDL and oxidized LDL (oxLDL), and cellular components such as monocytes (m), macrophages (M), foam cells (FC), and contractile and synthetic smooth muscle cells (CSMC and SSMC). We also include cytokines (C) and collagen fibres (Cg). All these substances undergo convection and diffusion and interact with each other, allowing us to describe the inflammatory process in the arterial wall using convection–diffusion–reaction equations. Initially, all the muscle cells in the arterial wall are contractile. Therefore, the only substance with an initial concentration in the arterial wall is CSMC.

Convection–diffusion–reaction equations describe the behaviour of cells and substances in the arterial wall:

$$\underbrace{\frac{\partial C_i}{\partial t}}_{Time} + \underbrace{\nabla \cdot (-D_i \nabla C_i)}_{Diffusion} + \underbrace{k_{lag,i} \cdot \boldsymbol{u_p} \cdot \nabla C_i}_{Convection} = \underbrace{f_{Ci}(\ldots, C_i, \ldots)}_{Source-sink} \tag{21}$$

where C_i is the concentration of the specified substance and D_i is its diffusion coefficient in the arterial wall. Due to the layered structure of the arterial wall, longitudinal and circumferential diffusion of substances within it is favoured over radial diffusion, making the diffusion process anisotropic. According to Yuan et al. (1991), the ratio of longitudinal to radial diffusion coefficients in the media layer of the arterial wall is approximately 3. Given the similar arrangement of the arterial layers in the longitudinal and circumferential directions, their diffusion coefficients are assumed to be equal. The first term in the equation captures the temporal changes in the concentration of the substance within the arterial wall. The subsequent terms account for its diffusion and convection within the wall. The reactive terms describe interactions between substances in the arterial wall, encompassing phenomena such as chemotaxis, proliferation, differentiation, apoptosis, degradation, and generation. These reactive terms, fC_i, vary for each substance considered, as detailed in Table 2. In this work, only LDL is considered to undergo convection due to its small size, while its oxidized form, as well as monocytes and macrophages, are only considered to undergo diffusion processes (Cilla et al., 2013).

2.6. Plaque growth

The volumetric growth of the arterial wall results from the collective contributions of various cells and substances involved in the inflammatory process. However, the impact of many of these components is negligible due to their small size. Therefore, only larger cells and collagen fibres are thought to contribute to plaque formation. Assuming isotropic plaque growth, the volumetric expansion attributable to atheroma plaque formation can be expressed as follows:

$$\nabla \cdot v = \frac{\partial C_{FC,w}}{\partial t} \cdot v_{FC} + \frac{\partial C_{SSMC,w}}{\partial t} \cdot v_{SSMC} + \frac{\partial C_{Cg,w}}{\partial t} \cdot \frac{1}{\rho_{Cg}}, \tag{22}$$

where $C_{i,w}$ is the concentration of each substance in the arterial wall. v_{FC} and v_{SSMC} are the volumes of a single FC and SSMC, respectively. Foam cells are assumed to be spherical, whereas synthetic smooth muscle cells are modelled as ellipsoids, so that their volumes can be easily calculated (Hernández-López et al., 2023).

2.7. Geometry and analysed scenarios

The model consists of an axisymmetric 2D representation of the coronary artery with a simplified cylindrical geometry, based on Olgac et al. (2008) and further studies by the same authors (Cilla et al., 2013; Hernández-López et al., 2023). This geometry includes a perturbation designed to produce a recirculation zone comparable to those at arterial bifurcations, used to simulate areas with varying WSS. As shown in Fig. 1, the geometry includes the monolayered wall and the lumen, treating the endothelium and the adventitia as membranes. As mentioned, an obstructive plaque disrupts blood flow, generating regions of low and high WSS downstream, which are conducive to new plaque formation in the low WSS areas (less than 1 Pa). Wentzel et al. (2012), Doriot et al. (2000). The considered single layer includes the intima and media layers, with a thickness of 0.56 mm according to Holzapfel et al. (2005).

To explore the effect of arterial wall deformations, the zero-pressure geometry is first calculated to derive the pressurized geometry at 70 mmHg internal pressure. Initially, the zero-pressure geometry has a lumen radius of 1.275 mm and a wall thickness of 0.375 mm. By applying inflation corresponding to a blood flow output pressure of 100 mmHg, the analysis geometry is obtained, characterized by a

Table 2
Summary of the transient inflammatory equations described in Eq. (21).

Substance	Source–sink
LDL	$-d_{LDL}C_{LDL,w}$
Oxidized LDL	$d_{LDL}C_{LDL,w}k_{(LDL-oxLDL)} - LDL_{ox,r}C_{oxLDL_{,w}}C_{M,w}$
Monocytes	$-d_m C_{m,w} - m_d C_{m,w}$
Macrophages	$d_m C_{m,w}k_{(m-M)} - \frac{LDL_{ox,r}}{n_{FC}} \cdot C_{oxLDL_{,w}}C_{M,w}$
Cytokines	$C_r C_{oxLDL_{,w}}C_{M,w} - d_c C_{c,w}$
CSMCs	$-C_{CSMC,w} \cdot S_r \cdot \left(\frac{C_{c,w}}{k_c \cdot C^{th}_{c,w} + C_{c,w}}\right)$
SSMCs	$C_{CSMC,w} \cdot S_r \cdot \left(\frac{C_{c,w}}{k_c \cdot C^{th}_{c,w} + C_{c,w}}\right) \cdot k_{(SMC)} + \left(\frac{p_{ss}C_{c,w}}{C^{th}_{c,w/2} + C_{c,w}}\right) C_{SSMC,w}\left(1 - \frac{C_{SSMC,w}}{C^{th}_{SSMC,w}}\right)$ $-r_{Apop} \cdot C_{SSMC,w}$
FCs	$\frac{LDL_{ox,r}}{n_{FC}} \cdot C_{oxLDL_{,w}}C_{M,w} \cdot k_{(M-FC)}$
Collagen	$G_r \cdot C_{SSMC,w} - d_{Cg} \cdot C_{Cg,w}$

wall thickness of 0.347 mm. Fig. 1 illustrates the arterial geometry pre-inflation (a) and post-inflation (b).

A comprehensive analysis of 10 distinct models is conducted. (i) Firstly, a baseline model is examined as detailed in the Geometry section. (ii) Second, a model is developed to investigate the impact of deformation from arterial wall inflation on plaque growth by adjusting its tortuosity. (iii) Third, another model explores changes in wall porosity due to inflation-induced deformations. Fourth, (iv) a model assesses changes in arterial wall permeability due to inflation-induced deformations. Lastly, (v) a model combines variations in tortuosity, permeability, and porosity. In total, five distinct scenarios will be explored. Additionally, (vi-x) these five scenarios will be evaluated under the influence of hypertension, varying the blood flow pressure from 100 mmHg to 160 mmHg.

2.8. Numerical methods

Finite element method was used to solve the mathematical model using COMSOL Multiphysics software (COMSOL AB, Burlington, MA, USA). The numerical solution involved four consecutive steps. First, the steady-state blood and plasma flows were calculated in two successive steps. Then, the inflammatory process within the arterial wall was simulated over a total period of 10 years. In the final step, the plaque growth at the tenth year was computed in a steady-state analysis. The computations were performed using the MUltifrontal Massively Parallel sparse direct Solver (MUMPS) for all stages of the model (Project-PARASOL, 1999). The inflammatory process was addressed in separate steps for different substances, and transient problems were solved using the Backwards Differentiation Formula (BDF) method, which is implicit and uses Newton's method for nonlinear problems (Curtiss and Hirschgelder, 1952; Gear, 1967).

A sensitivity analysis was conducted on the geometry length and mesh size, revealing that a minimum artery length of 90 mm ensured fully developed blood flow. Quadrilateral elements were used to mesh the model domains, incorporating three boundary layers near the endothelium in the lumen to ensure accuracy around the wall, which is crucial as WSS is the key stimulus variable in this model. Sensitivity analyses of both lumen and arterial wall meshes were performed to select the optimal mesh, balancing computational cost and result accuracy. The final mesh consisted in 54 200 elements for the lumen and 56 248 for the arterial wall, totalling 110 448 elements. P1-P1 elements were used for blood flow calculations, with linear interpolation for velocity and pressure within the arterial lumen. A sensitivity analysis was performed by progressively refining a coarse mesh until results varied by less than 5%. A similar refinement process was applied to the number of boundary layers in the lumen mesh. Linear and quadratic elements were used for the inflammatory processes in the arterial wall and plasma flow through the endothelium and plaque growth, respectively.

Table 3
Maximum values of arterial wall thickness increase (mm) and percentage of increase relative to the base case for all studied scenarios.

	100 mmHg		160 mmHg	
Base case	0.311604		1.48547	
Tortuosity	0.311565	0.01%	1.4689	1.1%
Porosity	0.312111	0.01%	1.58881	6.9%
Permeability	0.311604	0.0%	1.48547	0.0%
All	0.31206	0.14%	1.76191	18.6%

3. Results

The aim of this study was to investigate the influence of arterial wall deformations on atheroma plaque growth, with a particular focus on assessing the effects of tortuosity, arterial wall permeability and porosity under both normal arterial pressure and hypertension. The results obtained provide a detailed understanding of these factors and their relationship to atheroma plaque development in the arteries. Fig. 2 shows the radial deformation of the arterial wall after inflation (arterial wall pressure) under both normal and high blood pressure conditions. Radial deformation values for normal pressure are relatively small, especially when compared to those under hypertension. The negative sign of the radial deformation values indicates compression.

Fig. 3 shows the velocity and pressure distribution along the artery for normal (100 mmHg) and high (160 mmHg) blood pressure. As expected, pressure is different in both, but velocity also varies due to the change in the artery's radius, which is altered by the deformation of the arterial wall.

Table 3 presents the maximum increase in arterial wall thickness [mm] for each scenario studied. Minimal variations are observed among the different cases under normal pressure. However, the arterial wall mechanics significantly impact the hypertensive condition compared to normal blood pressure. The maximum increase in wall thickness for the hypertensive base case is 1.48 mm. This value rises to 1.58881 mm (a 6.9% increase) when only porosity is considered, and to 1.76191 mm (an 18.6% increase) when tortuosity, porosity, and permeability are included. The effect of hypertension on atheroma plaque growth is evident, as the maximum wall thickness increases more than fivefold from the normal pressure case to the hypertension one.

Fig. 4 shows the atheroma plaque growth over 30 years for all studied cases. The impact of tortuosity on plaque growth was initially examined. Although tortuosity can vary from case to case, it showed no significant effect on the final growth of atheroma plaque under normal blood pressure. A slight influence was observed in the hypertensive case. As mentioned above, arterial tortuosity affects the diffusion coefficients of LDL, oxidized LDL, monocytes, and macrophages. Despite potential variations, the results indicated that tortuosity did not significantly influence plaque formation. The LDL and oxLDL diffusion

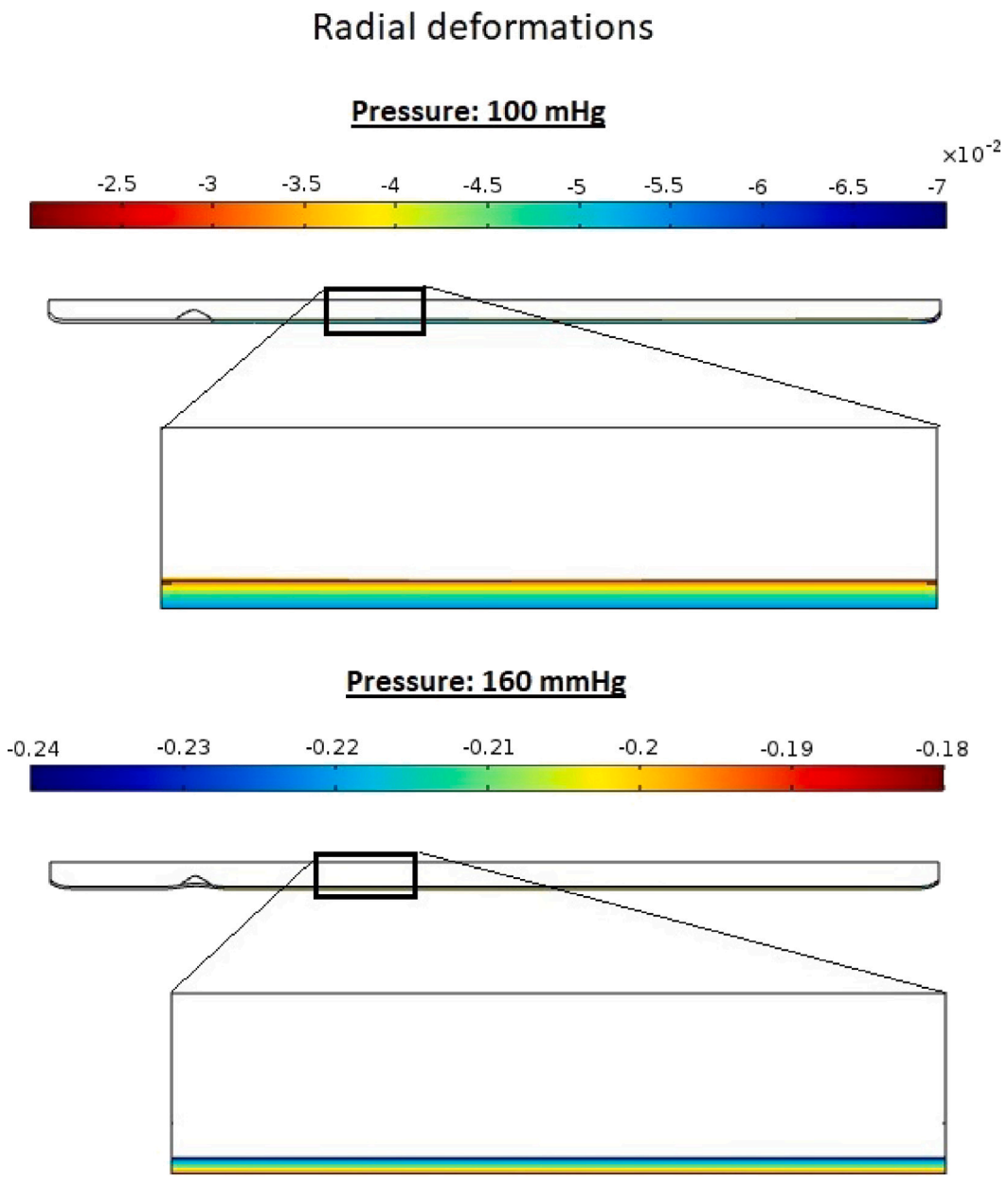

Fig. 2. Radial deformations for normal (100 mmHg) and high (160 mmHg) blood pressure.

coefficients for the base case are 8 10^{-13}, which only slightly change when accounting for arterial wall deformation.

The effect of arterial wall permeability on plaque growth was also assessed. The analyses showed that variations in wall permeability did not have a direct correlation with the final growth of atheroma plaque under normal or high blood pressure, as the permeability variations were minimal compared to the base case. Although permeability is an important factor in arterial fluid dynamics, the results suggest that it does not play a significant role in atheroma plaque development under these conditions.

The influence of porosity on plaque growth was also investigated. Results indicated that at normal blood pressure, arterial wall porosity had no significant impact on atheroma plaque growth. However, as arterial pressure increased, so did the influence of porosity on atheroma plaque growth. When considering all factors (tortuosity, porosity, and permeability), the effect of arterial wall deformations on atheroma plaque growth was more pronounced under hypertension.

Additionally, we examined the impact of hypertension, showing that the atheroma plaque growth increased approximately fivefold under high arterial pressure (Fig. 4).

Finally, Fig. 5 shows the temporal evolution of foam cells, smooth muscle cells and collagen, which are the key contributors to plaque growth. For cases with a blood pressure of 1100 mmHg, the evolution patterns are quite similar. However, significant differences are observed in the cases with a blood pressure of 160 mmHg.

4. Discussion

This study investigated the effect of hypertension on atherosclerotic plaque formation using a mechanobiological model. To accurately assess the effect of hypertension, the model was modified to include wall compression-induced packing, affecting diffusion, porosity and permeability. Analyses were performed by considering variations in all variables simultaneously and individually.

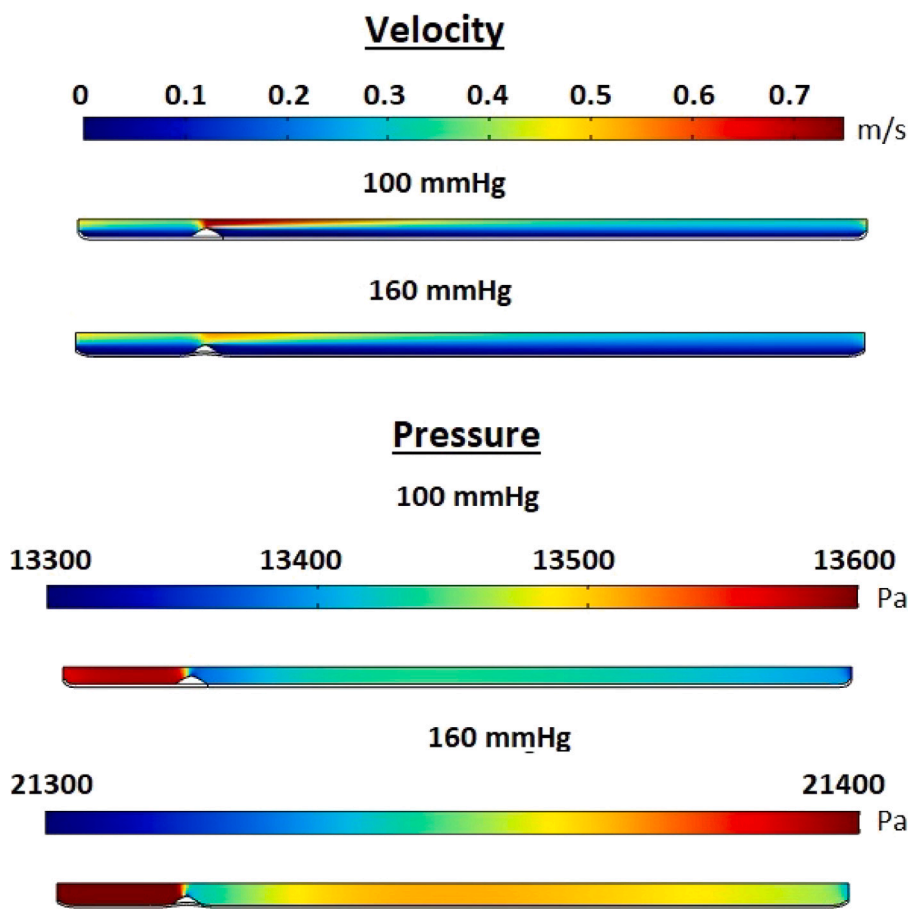

Fig. 3. Velocity and pressure for normal (100 mmHg) and high (160 mmHg) blood pressure.

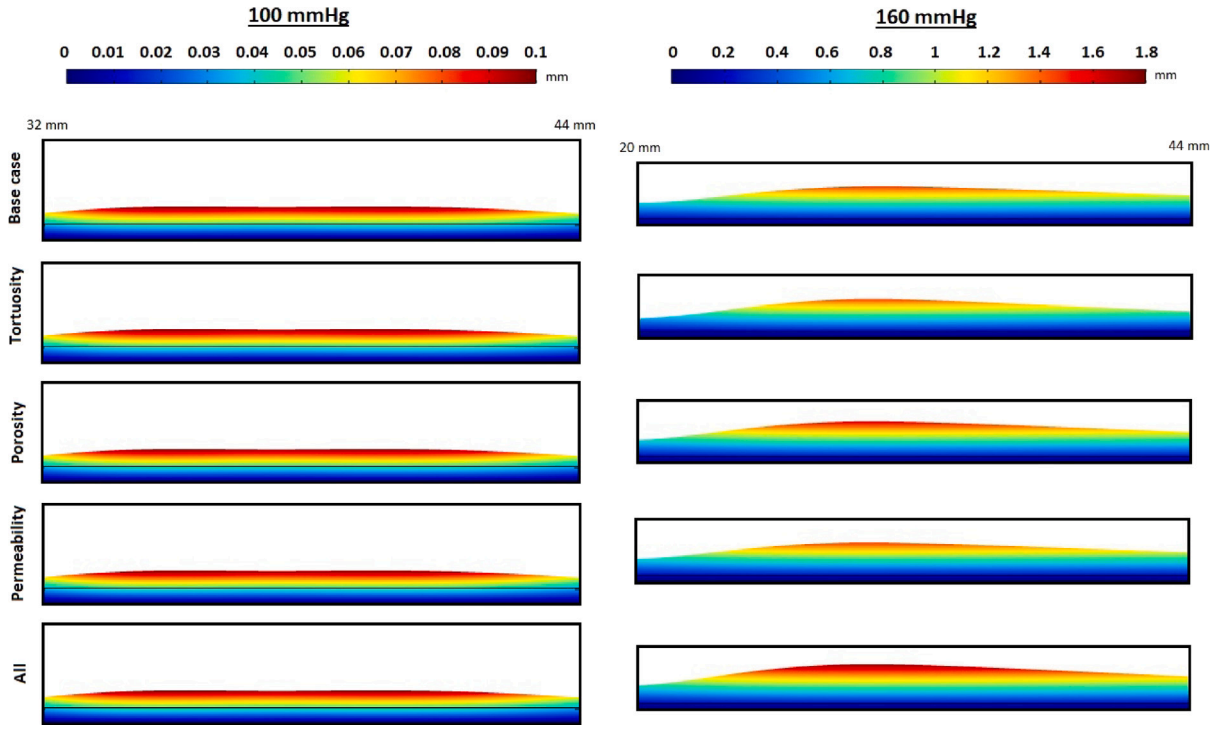

Fig. 4. Atheroma wall thickness increase for all studied scenarios (mm).

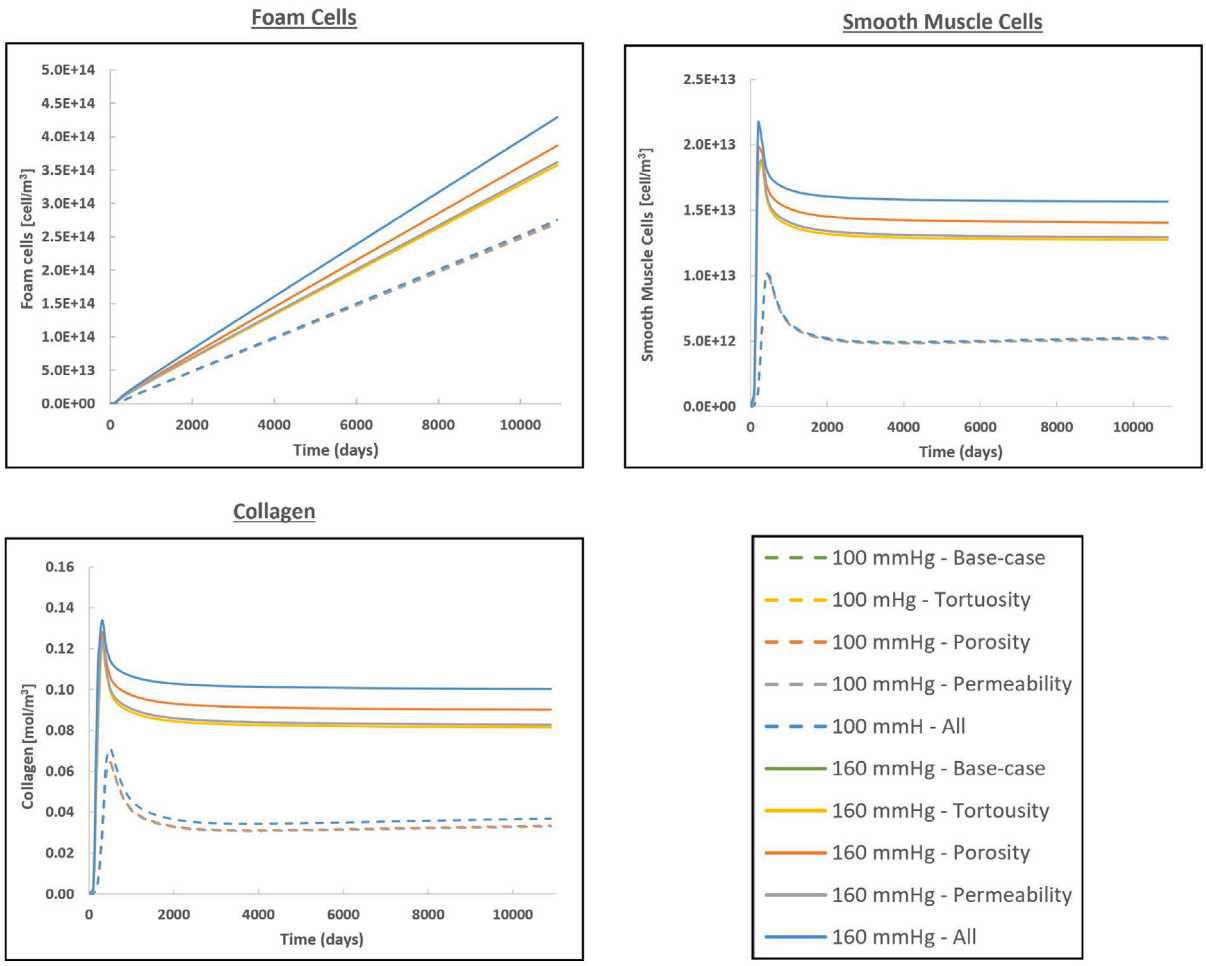

Fig. 5. Temporal evolution of Foam Cells, Smooth Muscle Cells and Collagen along the time.

As shown in Fig. 4 and Table 3, hypertension significantly affects the atheroma growth. This phenomenon is due to several factors discussed above. Primarily, the increase in lumen pressure leads to a substantial rise in wall pressure drop. Consequently, according to Darcy's law (Eq. (17)), J_v escalates, increasing the flow of LDL across the endothelium. This effect persists regardless of wall mechanics. Hypertension also impacts growth-associated substances (foam cells, SMCs and collagen), with increases of 60%, 300% and 225%, respectively. The greater rise in SMCs and collagen compared to foam cells may result from reduced diffusion under hypertension, leading to higher LDL concentrations near the lumen and increased cytokine levels, which attract SMCs from the media into the intima. This suggests a more fibrotic and stable plaque, less prone to rupture (Bentzon et al., 2014).

Interestingly, elevated blood pressure induces changes in both plaque position and morphology. The asymmetry of the plaque as well as the changes in the location of maximal growth in hypertensive cases could be attributed to increased radial deformation, which enlarges the lumen diameter. This dilation alters both the velocity and pressure profiles as shown in Fig. 3. Consequently, these events generate variations in the recirculation zone, affecting the region of lower wall shear stress (WSS) where the inflammatory process begins.

Regarding wall expansion, the results presented in Fig. 4 indicate a minimal influence on growth when considering wall mechanics under normotensive conditions (100 mmHg). This is due to the minor variation in radial strain along the wall, leading to limited effects in porosity, diffusion and permeability when using a constant mean strain value. However, under hypertensive conditions (160 mmHg), the impact is much more pronounced.

The effect of hypertension on wall compaction can be seen in Fig. 2. We observed that radial deformations increase by an order of magnitude when pressure rises to 160 mmHg. resulting in pronounced variations in material parameters along the wall. Consequently, including mechanical dependence in the growth model becomes crucial.

Both Fig. 4 and Table 3 indicate that mechanics primarily influence plaque growth via porosity, with lesser effects from permeability and tortuosity. Nevertheless, the combined effect of all these factors (tortuosity, permeability and porosity) increases plaque growth by almost 20% in hypertensive scenarios. This highlights the need to consider wall compression due to hypertension in patient-specific models, as elevated blood pressure often coexists with high cholesterol levels, significantly affecting plaque growth. Fig. 5 further illustrates that foam cells, SMCs, and collagen are unaffected by mechanics under normotensive conditions but show differences under hypertension, particularly in the long term. After 500 days, the difference between considering wall mechanics or not becomes apparent, and especially towards the end of the 30-year process. In the short term, however, this contrast is less pronounced.

The computational model has limitations. Firstly, the model only considers the primary substances involved in the atherosclerotic process, neglecting factors such as high-density lipoproteins, oxygen or metalloproteinases. Elevated blood pressure can induce structural changes in the arteries, such as thickening of the arterial walls (hypertrophy) and narrowing of the arterial lumen (stenosis). These changes can promote the accumulation of atheromatous plaque and obstruct blood flow. However, our current model does not include the effect of hypertrophy, which would alter the media structure and thus the

variables considered. Future work is expected to address this issue. Prolonged hypertension leads to endothelial damage through endothelial cell turnover. This effect could be implemented by modifying the leaky junctions fraction in the arterial wall (Φ_{lj}). However, apart from theoretical studies (Cancel et al., 2007), there is no available data that allows for the adjustment of Φ_{lj} with pressure. Finally, given the considerable computational demands of the model and since this study focuses on analysing the impact of artery wall mechanics on plaque growth, a 2D axisymmetric approximation was sufficient.

In conclusion, hypertension markedly accelerates plaque growth, resulting in a more than 400% increase in plaque thickness, independent of wall mechanics. While tortuosity, arterial wall permeability and porosity have minimal impact on plaque growth under normal arterial pressure, their combined influence under hypertension results in an almost 20% increase in plaque growth. This underscores the importance of considering wall compression due to hypertension in patient studies, where elevated blood pressure and high cholesterol levels often coexist.

CRediT authorship contribution statement

Patricia Hernández-López: Writing – review & editing, Methodology, Formal analysis. **Nicolás Laita:** Writing – review & editing, Formal analysis, Conceptualization. **Myriam Cilla:** Writing – original draft, Formal analysis, Conceptualization. **Miguel Ángel Martínez:** Writing – review & editing, Methodology, Funding acquisition, Formal analysis, Conceptualization. **Estefanía Peña:** Writing – review & editing, Methodology, Funding acquisition, Formal analysis, Conceptualization.

Declaration of competing interest

The authors declare that the research was conducted in the absence of any commercial or financial relationships that could be construed as a potential conflict of interest.

Acknowledgements

Support was obtained from the Spanish Ministry of Science and Technology through the research projects PID2019-107517RB-I00 and PID2022-140219OB-I00 and financial support to P. Hernández-López through the grant BES-2017-080239. This work has also been supported by the Government of Aragón), Spain through the T24-20R research project and by the Instituto de Salud Carlos III (ISCIII), Spain through the CIBER initiative. Myriam Cilla is supported by Grant Ramón y Cajal 171562 funded by MICIU/AEI/10.13039/501100011033 and the European Social Fund Plus (FSE+).

Appendix A. Plasma flow through the endothelium

The endothelium comprises tightly arranged cells structured to minimize intercellular spaces. According to the three-pore model, plasma flow across the endothelium results from the combined currents originating from three different sources: normal junctions, leaky junctions between endothelial cells and vesicular pathways (Olgac et al., 2008).

$$J_v = Jv_{nj} + Jv_{lj} + Jv_{vp} \tag{23}$$

The first flow (Jv_{nj}) occurs when the endothelium is healthy, while the second one (Jv_{lj}) occurs when there are leaky or pathological junctions. The third flow (Jv_{vp}) takes place across the endothelial cells through Vesicular Pathways. However, this plasma flow is much smaller compared to the other two and is considered negligible (Olgac et al., 2008).

To accurately determine plasma flow through the arterial wall, it is essential to have knowledge of the expressions corresponding to normal and leaky junction flows. The calculation of plasma flow through normal junctions can be achieved by:

$$Jv_{nj} = Lp_{nj} \cdot (\Delta P_{End} - \sigma_d \cdot \Delta\Pi) \cdot (1 - \Phi_{lj}), \tag{24}$$

where Lp_{nj} is the hydraulic conductivity of normal junctions. The value of Lp_{nj} depends on the thickness of the arterial wall and the intraluminal pressure (Tedgui and Lever, 1984). ΔP_{End} is the pressure drop across the endothelium, which depends on the intraluminal pressure and has values of 18 mmHg and 28 mmHg for intraluminal pressures of 70 mmHg and 180 mmHg respectively (Tedgui and Lever, 1984). The term $\sigma_d \cdot \Delta\Pi$ is related to osmotic pressure, where σ_d is the osmotic reflection coefficient of the plasma and $\Delta\Pi$ is the osmotic pressure difference across the endothelium. However, according to Tedgui and Lever (1984), the influence of the osmotic term is small compared to that of the hydrostatic pressure (Tedgui and Lever, 1984). Finally, Φ_{lj} is the fraction of leaky junctions in the arterial wall (Weinbaum et al., 1985; Huang et al., 1994; Huang and Tarbell, 1997). The ratio Φ_{lj} depends on the hemodynamics of the blood flow, for example the wall shear stress (WSS), through experimental correlations based on the endothelial cell shape index (SI).

Based on experimental data from Levesque et al. (1986), a relationship between the WSS of blood flow with the endothelium and the shape index of endothelial cells was considered (Hernández-López et al., 2023):

$$SI = 0.6296 \cdot e^{(-0.8709 \cdot WSS)} + 0.2145 \cdot e^{(-0.03938 \cdot WSS)} \tag{25}$$

It is well accepted that low wall shear stress (WSS) regions are prone to atherosclerosis, whereas regions of high WSS are protective against atherosclerosis. Specifically for the carotid arteries, regions below 2, Pa are prone to atheroma plaque formation (Younis et al., 2004; Zhao et al., 2002).

The number of endothelial mitotic cells (MC) in areas of known shape index was determined (Chien, 2003), so the next experimental correlation was developed for an unit area of 0.64 mm^2 (Olgac et al., 2008).

$$MC = 0.003797 \cdot e^{(14.75 \cdot SI)}, \tag{26}$$

and the relation between the number of leaky and mitotic cells can be calculated as (Olgac et al., 2008):

$$LC = 0.307 + \frac{0.805 \cdot MC}{0.453} \tag{27}$$

Finally, Φ_{lj} is defined as the ratio between the area of leaky cells and the total area of the endothelium (Weinbaum et al., 1985; Huang et al., 1994; Huang and Tarbell, 1997; Olgac et al., 2008).

On the other hand, the flow of the plasma through the leaky junctions can be defined as follows

$$Jv_{lj} = Lp_{lj} \cdot (\Delta P_{End} - \sigma_d \cdot \Delta\Pi), \tag{28}$$

where, as in normal junctions, ΔP_{End}, σ_d and $\Delta\Pi$ are respectively the pressure drop across the endothelium, the osmotic reflection coefficient and the osmotic pressure difference across the endothelium (negligible according to Tedgui and Lever (1984)). Finally, Lp_{lj} is the hydraulic conductivity of the leaky junction, which can be calculated (Weinbaum et al., 1985; Huang et al., 1994; Huang and Tarbell, 1997; Olgac et al., 2008).

$$Lp_{lj} = \frac{4w_l}{R_{cell}} \cdot \Phi_{lj} \cdot \frac{w_l^2}{3 \cdot \mu_p \cdot l_{lj}} \tag{29}$$

where R_{cell} is the radius of the endothelial cells, which has a value of 15 μm and w_l is the half-width of a leaky junction, 20 nm (Weinbaum et al., 1985), μ_p and w_l are the dynamic viscosity of the plasma and the width of a leaky junction, respectively. Finally, l_{lj} is the length of a leaky junction in the plane perpendicular to the endothelial membrane 2 μm (Weinbaum et al., 1985).

Appendix B. LDL flow through the endothelium

As with plasma flow, LDL flow across the endothelium can be modelled using the three-pore model (Olgac et al., 2008). Molecules are

also transported across the endothelium in different ways depending on their size: through normal and leaky junctions and vesicular pathways:

$$Js = Js_{nj} + Js_{lj} + Js_{vp} \tag{30}$$

LDL flow through each of the possible pathways in the endothelium can be calculated using the classical Kedem–Katchalsky equation (Kedem and Katchalsky, 1958):

$$Js, i = C_{LDLdep} \cdot P_{app,i}\,, \tag{31}$$

being C_{LDLdep} the concentration of LDL molecules deposited in the arterial wall and $P_{app,i}$ is the apparent permeability coefficient of the arterial wall, which can be related to normal junctions, leaky junctions and vesicular pathways ($P_{app,nj}$, $P_{app,lj}$ and $P_{app,vp}$, respectively) according to the three-pore model. For molecules smaller than 2 nm, transport through all pathways is possible, but for larger molecules, which is the case of LDL whose radius is about 11 nm (Tarbell, 2003), transport through normal junctions is not possible, so in this case molecular transport across the endothelium occurs only through leaky junctions and vesicular pathways (Ogunrinade et al., 2002).

According to Cancel et al. (2007), molecular transport of LDL through vesicular pathways corresponds to the 10% of the flow through leaky junctions. Therefore:

$$P_{app,vp} = 0.1 \cdot P_{app,lj} = 0.1(P_{lj} Z_{lj} + J_{v,lj} \cdot (1 - \sigma_{f,lj}),) \tag{32}$$

where P_{lj}, Z_{lj} and $\sigma_{f,lj}$ are, respectively, the diffusive permeability of leaky junctions, a reduction factor of LDL concentration gradient at the entrance of the flow, and the solvent-drag coefficient of leaky junctions (Patlak et al., 1963; Tarbell, 2003). So, LDL flow across the endothelium can be written as:

$$J_{S,LDL} = 1.1 \cdot C_{LDLdep} \cdot (P_{lj} Z_{lj} + J_{v,lj}(1 - \sigma_{f,lj})) \tag{33}$$

The diffusive permeability of leaky junctions is defined as (Olgac et al., 2008):

$$P_{lj} = \frac{A_p}{S} P_{slj}(1 - \alpha_{lj}), \tag{34}$$

where P_{slj} is the permeability of a single leaky junction, α_{lj} is the fraction of the pore area occupied by LDL molecules, and can be calculated as the ratio of the radius of an LDL molecule (R_{LDL}) to the half-width of a leaky junction (w_l) (Olgac et al., 2008).

On the other hand, P_{slj} can be calculated with the diffusion coefficient of LDL in a leaky junction (D_{lj}) and the length of a leaky junction (l_{lj}):

$$P_{slj} = \frac{D_{lj}}{l_{lj}}, \tag{35}$$

where the diffusion coefficient of LDL in a leaky junction is related to the LDL diffusion coefficient in the arterial wall of the hole with an empirical correlation, see Olgac et al. (2008) and Renkin (1954).

The reduction factor of LDL concentration gradient, Z_{lj}, is a concentration reduction factor at the entrance of the pores of biological membranes, and it can be calculated as (Tarbell, 2003):

$$Z_{lj} = \frac{Pe_{lj}}{e^{(Pe_{lj})} - 1}, \tag{36}$$

which depends on a modified Peclet number for membranes. This modified Peclet number relates convective and diffusive processes of transport and is defined as (Tarbell, 2003):

$$Pe_{lj} = \frac{Jv, lj \cdot (1 - \sigma_{f,lj})}{P_{lj}} \tag{37}$$

Finally, $\sigma_{f,lj}$ is the solvent drag reflection coefficient of leaky junctions. It is a parameter that determines the selectivity of the endothelium for substances entering the arterial wall. Molecules with a reflection coefficient greater than one are excluded by the endothelium and cannot enter the arterial wall, see Olgac et al. (2008).

References

Ai, L., Vafai, K., 2006. A coupling model for macromolecule transport in a stenosed arterial wall. Int. J. Heat Mass Transfer 49 (9), 1568–1591.

Bentzon, J.F., Otsuka, F., Virmani, R., Falk, E., 2014. Mechanisms of plaque formation and rupture. Circ. Res. 114 (12), 1852–1866.

Brown, A.J., Teng, Z., Evans, P.C., Gillard, J.H., Samady, H., Bennett, M.R., 2016. Role of biomechanical forces in the natural history of coronary atherosclerosis. Nat. Rev. Cardiol. 13 (4), 210–220.

Budu-Grajdeanu, P., Schugart, R.C., Friedman, A., Valentine, C., Agarwal, A.K., Rovin, B.H., 2008. A mathematical model of venous neointimal hyperplasia formation. Theor. Biol. Med. Model. 5 (2), 1–9.

Bulelzai, M.A.K., Dubbeldam, J.L.A., 2012. Long time evolution of atherosclerotic plaques. J. Theoret. Biol. 297, 1–10.

Cancel, L.M., Fitting, A., Tarbell, J.M., 2007. In vitro study of LDL transport under pressurized (convective) conditions. Am. J. Physiol. - Heart Circ. Physiol. 293 (1), 126–132.

Caro, C., Pedley, T., Schroter, R., Seed, W., 1978. The Mechanics of the Circulation. Oxford University Press, Oxford.

Chien, S., 2003. Molecular and mechanical bases of focal lipid accumulation in arterial wall. Prog. Biophys. Mol. Biol. 83 (2), 131–151.

Cilla, M., Peña, E., Martínez, M.A., 2012. 3D computational parametric analysis of eccentric atheroma plaque: influence of axial and circumferential residual stresses. Biomech. Model. Mechanobiol. 11 (7), 1001–1013.

Cilla, M., Peña, E., Martínez, M.A., 2013. Mathematical modelling of atheroma plaque formation and development in coronary arteries. J. R. Soc. Interface 11 (90), 20130866.

Cunningham, K.S., Gotlieb, A.I., 2005. The role of shear stress in the pathogenesis of atherosclerosis. Lab. Invest. 85 (1), 9–23.

Curry, F., Michel, C., 1980. A fiber matrix model of capillary permeability. Microvasc. Res. 20 (1), 96–99.

Curtiss, C.F., Hirschgelder, J.O., 1952. Integration of Stiff equations. Proc. Natl. Acad. Sci. 38 (3), 235–243.

Dabagh, M., Jalali, P., Tarbell, J.M., 2009. The transport of LDL across the deformable arterial wall: The effect of endothelial cell turnover and intimal deformation under hypertension. Am. J. Physiol. - Heart Circ. Physiol. 297 (3), 983–996.

Denny, W.J., O'Connell, B.M., Milroy, J., Walsh, M.T., 2012. An analysis of three dimensional diffusion in a representative arterial wall mass transport model. Ann. Biomed. Eng. 41 (5), 1062–1073.

Denny, W.J., Walsh, M.T., 2014. Numerical modelling of mass transport in an arterial wall with anisotropic transport properties. J. Biomech. 47 (1), 168–177.

Doriot, P.A., Dorsaz, P.A., Dorsaz, L., De Benedetti, E., Chatelain, P., Delafontaine, P., 2000. In-vivo measurements of wall shear stress in human coronary arteries. Coron. Artery Dis. 11 (6), 495–502.

Elishaev, M., Hodonsky, C.J., Ghosh, S.K.B., Finn, A.V., von Scheidt, M., Wang, Y., 2022. Opportunities and challenges in understanding atherosclerosis by human biospecimen studies. Front. Cardiovascul. Med. 7 (9), 948492.

Filipovic, N., Teng, Z., Radovic, M., Saveljic, I., Fotiadis, D., Parodi, O., 2013. Computer simulation of three-dimensional plaque formation and progression in the carotid artery. Med. Biol. Eng. Comput. 51 (6), 607–616.

Gear, C.W., 1967. The numerical integration of ordinary differential equations. Math. Comp. 21 (98), 146–156.

Gusev, E., Sarapultsev, A., 2023. Atherosclerosis and inflammation: Insights from the theory of general pathological processes. Int. J. Mol. Sci. 24 (9), 7910.

Hernández-López, P., Cilla, M., Martínez, M.A., Peña, E., 2021. Effects of the haemodynamic stimulus on the location of carotid plaques based on a patient-specific mechanobiological plaque atheroma formation model. Front. Bioeng. Biotechnol. 9 (30), 690685, URL https://www.frontiersin.org/articles/10.3389/fbioe.2021.690685.

Hernández-López, P., Martínez, M.A., Peña, E., Cilla, M., 2023. Understanding the parameter influence on lesion growth for a mechanobiology model of atherosclerosis. Mathematics 11 (4), 829, URL https://www.mdpi.com/2227-7390/11/4/829.

Holzapfel, G.A., Sommer, G., Gasser, C.T., Regitnig, P., 2005. Determination of layer-specific mechanical properties of human coronary arteries with nonatherosclerotic intimal thickening and related constitutive modeling. Am. J. Physiol.-Heart Circ. 289 (5), H2048–H2058.

Huang, Y., Jan, K.M., Rumschitzki, D., Chien, S., S., W., 1998. Structural changes in rat aortic intima due to transmural pressure. J. Biomech. Eng. 120 (1), 476–483.

Huang, Y., Rumschitzki, D., Chien, S., Weinbaum, S., 1992. A fiber matrix model for the growth of macromolecular leakage spots in the arterial intima. Adv. Biol. Heat Mass Transf. 231 (1), 81–92.

Huang, Y., Rumschitzki, D., Chien, S., Weinbaum, S., 1994. A fiber matrix model for the growth of macromolecular leakage spots in the arterial intima. J. Biomech. Eng. 116 (4), 430–445.

Huang, Z., Tarbell, J., 1997. Numerical simulation of mass transfer in porous media of blood vessel walls. Am. J. Physiol.-Heart Circ. Physiol. 273 (1), H464–H477.

Humphrey, J.D., 2002. Cardiovascular Solid Mechanics: Cells, Tissues and Organs. Springer-Verlag, New York.

Jesionek, K., Slapik, A., Kostur, M., 2016. Low-density lipoprotein transport through an arterial wall under hypertension - A model with time and pressure dependent fraction of leaky junction consistent with experiments. J. Theoret. Biol. 411 (1), 81–91.

Kedem, O., Katchalsky, A., 1958. Thermodynamic analysis of the permeability of biological membranes to non-electrolytes. Biochim. Biophys. Acta 27 (2), 229–246.

Levesque, M.J., Liepsch, D., Moravec, S., Nerem, R.M., 1986. Correlation of endothelial cell shape and wall shear stress in a stenosed dog aorta. Am. Heart Assoc. J. 6, 220–229.

Libby, P., Aikawa, M., 2002. Stabilization of atherosclerotic plaques: New mechanisms and clinical targets. Nat. Med. 8 (11), 1257–1262.

Liu, Y., Luo, X., Jia, H., Yu, B., 2022. The effect of blood pressure variability on coronary atherosclerosis plaques. Front. Cardiovascul. Med. 9 (1), 803810.

Malvè, M., Chandra, S., García, A., Mena, A., Martínez, M.A., Finol, E.A., Doblaré, M., 2014. Impedance-based outflow boundary conditions for human carotid haemodynamics. Comput. Methods Biomech. Biomed. Eng. 17 (11), 1248–1260.

Meyer, G., Merval, R., Tedgui, A., 1996. Effects of pressure-induced stretch and convection on low-density lipoprotein and albumin uptake in the rabbit aortic wall. Circ. Res. 79 (3), 532–540.

Nolan, D.R., McGarry, J.P., 2016. On the compressibility of arterial tissue. Ann. Biomed. Eng. 44 (4), 993–1007.

Ogunrinade, O., Kameya, G.T., Truskey, G.A., 2002. Effect of fluid shear stress on the permeability of the arterial entohelium. Ann. Biomed. Eng. 30, 430–446.

Olgac, U., Kurtcuoglu, V., Poulikakos, D., 2008. Computational modeling of coupled blood-wall mass transport of LDL: Effects of local wall shear stress. Am. J. Physiol. - Heart Circ. Physiol. 294 (2), 909–919.

Olivares, A., González Ballester, M., Noailly, J., 2016. Virtual exploration of early stage atherosclerosis. Bioinformatics 32 (24), 3798–3806.

Pappalardo, F., Musumeci, S., Motta, S., 2008. Modeling immune system control of atherogenesis. Bioinformatics 24 (15), 1715–1721.

Patlak, C.S., Goldstein, D.A., Hoffman, J.F., 1963. The flow of solute and solvent across a two-membrane system. J. Theoret. Biol. 5 (3), 426–442.

Perktold, K., Resch, M., Florian, H., 1991. Pulsatile non-newtonian flow characteristics in a three-dimensional human carotid bifurcation model. J. Biomech. Eng. 113 (4), 464–475.

Project-PARASOL, 1999. CERFACs, IRIT-ENSEEIHT, and RAL. Multi-frontal massively parallel sparse direct solver, MUMPS. URL https://mumps-solver.org.

Prosi, M., Zunino, P., Perktold, K., Quarteroni, A., 2005. Mathematical and numerical models for transfer of low-density lipoproteins through the arterial walls: A new methodology for the model set up with applications to the study of disturbed lumenal flow. J. Biomech. 38 (4), 903–917.

Renkin, E.M., 1954. Filtration, diffusion, and molecular sieving through porous cellulose membranes. J. Gen. Physiol. 38 (2), 225–243.

Schwenke, D.C., Carew, T.E., 1989. Initiation of atherosclerotic lesions in cholesterol-fed rabbits. II. selective retention of LDL vs. selective increases in LDL permeability in susceptible sites of arteries. Arteriosclerosis 9 (6), 908–918.

Sun, N., Wood, N.B., Hughes, A.D., Thom, S.A.M., Xu, X.Y., 2007. Effects of transmural pressure and wall shear stress on LDL accumulation in the arterial wall: A numerical study using a multilayered model. Am. J. Physiol. - Heart Circ. Physiol. 292 (6), 3148–3157.

Tarbell, J.M., 2003. Mass transport in arteries and the localization of atherosclerosis. Annu. Rev. Biomed. Eng. 5 (1), 79–118.

Tedgui, A., Lever, M.J., 1984. Filtration through damaged and undamaged rabbit thoracic aorta. Am. J. Physiol.-Heart Circ. Physiol. 247 (5), H784–H791.

Truskey, G., Roberts, W., Herrmann, R., Malinauskas, R., 1992. Measurement of endothelial permeability to 125I-low density lipoproteins in rabbit arteries by use of en face preparations. Circ. Res. 71 (1), 883–897.

VanEpps, J.S., Vorp, D.A., 2007. Mechanopathobiology of atherogenesis: A review. J. Surg. Res. 142 (1), 202–2017.

Virani, S., Alonso, A., Aparicio, H., Benjamin, E., Bittencourt, M., Callaway, C., Carson, A., Chamberlain, A., Cheng, S., Delling, F., Elkind, M., Evenson, K., Ferguson, J., Gupta, D., Khan, S., Kissela, B., Knutson, K., Lee, C., Lewis, T., Liu, J., Loop, M., Lutsey, P., Ma, J., Mackey, J., Martin, S., Matchar, D., Mussolino, M., Navaneethan, S., Perak, A., Roth, G., Samad, Z., Satou, G., Schroeder, E., Shah, S., Shay, C., Stokes, A., VanWagner, L., Wang, N., Tsao, C., 2021. Heart disease and stroke statistics-2021 update: A report from the American heart association. Circulation 143 (8), e254–e743.

Wang, H., Patterson, C., 2015. Atherosclerosis: Risks, Mechanisms, and Therapies. Wiley-Blackwell, Nueva Jersey.

Weinbaum, S., Tzeghai, G., Ganatos, P., Pfeffer, R., Chien, S., 1985. Effect of cell turnover and leaky junctions on arterial macromolecular transport. Am. J. Physiol.-Heart Circ. Physiol. 248 (6), H945–H960.

Wentzel, J.J., Chatzizisis, Y.S., Gijsen, F.J., Giannoglou, G.D., Feldman, C.L., Stone, P.H., 2012. Endothelial shear stress in the evolution of coronary atherosclerotic plaque and vascular remodelling: current understanding and remaining questions. Cardiovascul. Res. 96 (2), 234–243.

Yeoh, O.H., 1993. Some forms of the strain energy function for rubber. Rubber Chem. Technol. 66 (5), 754–771.

Younis, H.F., Kaazempur-Mofrad, M.R., Chan, R.C., Isasi, A.G., Hinton, D.P., Chau, A.H., Kim, L.A., Kamm, R.D., 2004. Hemodynamics and wall mechanics in human carotid bifurcation and its consequences for atherogenesis: Investigation of inter-individual variation. Biomech. Model. Mechanobiol. 3 (1), 17–32.

Yuan, F., Chien, S., Weinbaum, S., 1991. A new view of convective-diffusive transport processes in the arterial intima. J. Biomech. Eng. 113 (3), 314–329.

Zhao, S.Z., Ariff, B., Long, Q., Hughes, A.D., Thom, S.A., Stanton, A.V., Xu, X.Y., 2002. Inter-individual variations in wall shear stress and mechanical stress distributions at the carotid artery bifurcation of healthy humans. J. Biomech. 35 (10), 1367–1377.